ENVIRONMENTAL RESEARCH
CLIMATE

PURPOSE-LED PUBLISHING™

PAPER • OPEN ACCESS

Evaluation of historical precipitation interannual variability in CMIP6 over the United States

To cite this article: Ryan D Harp *et al* 2024 *Environ. Res.: Climate* **3** 045032

ENVIRONMENTAL RESEARCH
CLIMATE

OPEN ACCESS

RECEIVED
10 June 2024

REVISED
27 November 2024

ACCEPTED FOR PUBLICATION
19 December 2024

PUBLISHED
2 January 2025

PAPER

Evaluation of historical precipitation interannual variability in CMIP6 over the United States

Ryan D Harp[1,4], **Thierry N Taguela**[2,4,*], **Akintomide A Akinsanola**[2,3] and **Daniel E Horton**[1]

[1] Department of Earth, Environmental, and Planetary Sciences, Northwestern University, Evanston, IL, United States of America
[2] Department of Earth and Environmental Sciences, University of Illinois Chicago, Chicago, IL, United States of America
[3] Environmental Science Division, Argonne National Laboratory, Lemont, IL, United States of America
[4] Contributed equally.
[*] Author to whom any correspondence should be addressed.

E-mail: taguela@uic.edu

Keywords: United States, precipitation, interannual variability, CMIP6 models, internal variability

Supplementary material for this article is available online

Abstract

Interannual precipitation variability profoundly influences society via its effects on agriculture, water resources, infrastructure, and disaster risks. In this study, we use daily *in situ* precipitation observations from the global historical climatology network-daily (GHCN-D) to assess the ability of 21 Coupled Model Intercomparison Project Phase 6 (CMIP6) models, including the 50-member fifth-generation Canadian Earth System Model single model initial-condition large ensemble (CanESM5_SMILE), to realistically simulate historical interannual precipitation variability trends within 17 regions of the contiguous United States (CONUS). We assess how accurately the CMIP6 simulations align with observational data across annual, summer, and winter periods, focusing on four key hydrometeorological metrics, including interannual precipitation variability, relative interannual precipitation variability (coefficient of variation), annual mean precipitation, and annual wet day frequency. Our findings reveal that CMIP6 ensemble members generally reproduce the spatial patterns of observed trends in annual mean precipitation. In most regions, models agree well with the signs of observed changes in annual mean precipitation, though discrepancies in trend magnitude are evident. Further, observed trends in winter mean precipitation broadly exhibit a spatial pattern similar to that of the observed annual mean. However, analysis of the CanESM5_SMILE shows that trends in precipitation variability may primarily be the result of model-simulated internal variability, suggesting caution in interpreting multi-model single-realization ensemble results. Challenges in accurately simulating interannual precipitation variability underscore the need for ongoing model refinement and validation to enhance climate projections, especially in regions vulnerable to extreme precipitation events.

1. Introduction

Understanding precipitation variability—the deviation of precipitation at different timescales from the mean state (Akinsanola *et al* 2020a)—plays a crucial role in the effective management of water resources and in safeguarding against successive hydrological extremes (Masson-Delmotte *et al* 2021). For instance, precipitation variabilities at daily-to-decadal timescales have been linked to catastrophic successive extreme events, including large-scale droughts and floods (e.g. Li *et al* 2013, Stevenson *et al* 2015). Precipitation variability is also tied to significant impacts on food security through altered streamflow and increased drought incidence, leading to decreased crop yields (Riha *et al* 1996, Barlow *et al* 2001, Abghari *et al* 2013). The United States (U.S.) has experienced a series of unusual droughts and flood events in recent decades (Griffin and Anchukaitis 2014, Corringham *et al* 2019), many of which have caused hundreds of millions of dollars in damages. Rising population, increased development, and climate change will worsen the risk

associated with hydrometeorological events in future decades (Masson-Delmotte *et al* 2021, Furtak and Wolińska 2023). Therefore, an improved understanding of precipitation variability and related trends, especially at regional scales, is crucial for informing accurate policy and management decisions. This is particularly true for sectors geared toward adapting to imminent hydrometeorological threats (Wood and Ludwig 2020, Wood *et al* 2021) through agricultural planning practices, water resource management, infrastructure planning, and disaster risk reduction.

Several studies have examined historical precipitation characteristics, including precipitation variability, over the U.S. instrumental record. Most of them reported a decrease in mean precipitation over the southwestern U.S. but increased precipitation over the Midwest and Great Plains (Nash *et al* 2017, Harp and Horton 2023). These findings are consistent with a general drying trend over the western U.S. since the 1970s, especially in the southwest, where mild to extreme drought has persisted for the past four decades (Peterson *et al* 2013, Williams *et al* 2022). Similarly, the frequency and intensity of extreme precipitation events have also increased in many parts of the country (Karl and Knight 1998, Alexander *et al* 2006, Groisman *et al* 2012). For instance, the Northeast, Great Plains, Midwest, and Southeast of the U.S. have experienced a significant increase in the number and intensity of heavy precipitation events in recent decades (Kunkel *et al* 2013, Nash *et al* 2017, Harp and Horton 2022). On the other hand, interannual precipitation variability has exhibited diverse changes, with rising variability in the southeast, a decline in the far west, and mixed signals in the Rocky Mountains and north-central U.S. (Harp and Horton 2023). These observed changes in precipitation characteristics have implications for flooding, water resource management, and ecosystem dynamics.

In general, recent changes in precipitation have been linked to greater moisture availability associated with rising global temperatures (i.e. the Clausius–Clapeyron relationship) and altered large-scale atmospheric circulations caused by climate change (e.g. Polade *et al* 2014), with the planetary energy budget setting the boundaries for precipitation changes (Pendergrass and Hartmann 2014). Global circulation models have been widely used to understand historical and future changes in climate phenomena at global and regional scales. Moreover, outputs from these models are increasingly applied beyond the scientific domain, particularly within climate impact assessments and decision-making processes (Rowell 2019, Akinsanola *et al* 2020b, Masson-Delmotte *et al* 2021, U.S. Global Change Research Program 2023). Therefore, a thorough evaluation of model performance is imperative. Coupled Model Intercomparison Project Phase 6 (CMIP6) represents the latest generation of climate models (Eyring *et al* 2016) coordinated by the World Climate Research Programme (WCRP). Previous studies focused on the U.S. have assessed the performance of CMIP6 models in simulating precipitation characteristics such as, but not limited to, mean climatology (Rivera and Arnould 2020) and extreme events (Srivastava *et al* 2020, Akinsanola *et al* 2020c). To build on these efforts, and informed by recent characterizations of observed changes in variability by Harp and Horton (2023), we aim to assess the performance of CMIP6 models with a focus on their ability to reproduce observed historical changes in the interannual precipitation variability across the contiguous U.S. (CONUS).

As such, the goal of this study is to perform a regionally-focused assessment of the changes in interannual precipitation variability across the CONUS in CMIP6 model simulations of the historical period (i.e. 1951–2014). Our analysis explores the following questions: (1) How does the magnitude of annual and seasonal variability simulated by the CMIP6 models compare to observed values across the CONUS? (2) How do trends of observed and CMIP6-simulated precipitation variability vary spatially across CONUS? (3) What context can the CanESM5_SMILE-simulated internal variability provide regarding trends identified in the CMIP6 multi-model single-realization ensemble?

2. Data and methods

The historical (1951–2014) daily precipitation datasets assessed in this study are sourced from CMIP6 model simulations (Eyring *et al* 2016). Building upon the successes of previous phases, CMIP6 aims to improve the realism and fidelity of climate simulation output over previous phases. This is achieved through advancements in model physics, parameterizations, and higher resolutions (Eyring *et al* 2016, Meehl *et al* 2020). Moreover, while previous phases predominantly relied on representative concentration pathways (RCPs) as the framework for emission scenarios, CMIP6 has embraced shared socioeconomic pathways (SSPs), which amalgamate both greenhouse gas emissions and socioeconomic variables. Through coordinated experiments and standardized protocols, CMIP6 facilitates the comparison of model outputs and the assessment of model performance and uncertainties across different scenarios and periods (Eyring *et al* 2016). Previous studies have shown that, in the historical framework, climate model uncertainties are of two types: internal variability and model (or structural) uncertainty (Lehner *et al* 2020, Qiu *et al* 2024). Model uncertainty arises from the fact that different climate models simulate complex processes differently, e.g. cloud formation and ocean-atmosphere interactions and feedback mechanisms. In contrast, natural

fluctuations within the climate system cause internal variability. In this study, we explore uncertainties associated with the structural uncertainties of models by employing a 21-member multi-model single realization ensemble, hereafter referred to as the CMIP6 multi-model ensemble, and uncertainties associated with model-simulated internal variability using the 50-member CanESM5 single model initial-condition large ensemble (SMILE). Details (names, respective institutions, and spatial resolutions) of the 21-member CMIP6 multi-model ensemble are described in table S1. The selection of the 21 CMIP6 models was based on their use in Akinsanola *et al* (2020), which evaluated the performance of CMIP6 models in simulating seasonal extreme precipitation indices across the U.S. Construction of our CMIP6 multi-model ensemble follows guidance from the Intergovernmental Panel on Climate Change (IPCC) Sixth Assessment Report (AR6) (Masson-Delmotte *et al* 2021). A single realization from each model's simulation of the historical period is utilized, i.e. the first member (r1i1p1f1). Selecting a single member ensures equal treatment and weighting for all models, and practically speaking, the first realization (i.e. r1) is consistently available from all modeling groups, thus providing the most comprehensive multi-model ensemble.

To examine the influence of internal variability, we use the 50-member CanESM5_SMILE. We chose CanESM5 because it had the most realizations available at the time of analysis. CanESM5 is a fully coupled ocean-atmosphere-land-sea ice climate model (Swart *et al* 2019) consisting of 50 ensemble members with 165 yr integrations from 1850 to 2014. Owing to the experimental design, differences between individual SMILE realizations are solely attributed to internally generated climate variability. Using first-order conservative remapping, all model data are gridded onto a spatial grid of $2.81° \times 2.81°$ (the lowest model resolution) to ensure consistency and facilitate comparison across all model datasets. This is a commonly used best practice in the literature (e.g. Srivastava *et al* 2020, Akinsanola *et al* 2020c, Taguela *et al* 2022, Bobde *et al* 2024).

Daily *in situ* precipitation observations from the Global Historical Climatology Network daily (GHCN-D) are employed to provide verification data for the model outputs. Compiled by NOAA's National Centers for Environmental Information, the GHCN-D database encompasses records from over 2,000 stations across the U.S., constituting the most comprehensive collection of daily U.S. data available (Menne *et al* 2012). GHCN-D observations, sensitive to 0.1 mm, undergo 19 quality control tests to identify duplicate data, climatological outliers, and other inconsistencies (Durre *et al* 2010). We limit our set of GHCN-D station observations to data suitable for long-term trend analysis by requiring station records to possess 90% or more complete station-years to qualify, where we define a complete station-year as having 90% or more of all potential daily observations. Rather than analyzing station records individually, spatial aggregation is employed to provide a larger sample size and a more comprehensive regional view of change over time, given the inherent limitations of individual station statistics and internal climate variability. Our analysis is focused on the contiguous U.S. and is conducted over 17 domains delineated by the National Ecological Observatory Network (NEON; figure S1). These domains, designed to be climatically homogeneous, were established using temperature- and precipitation-informed geographic clustering (National Ecological Observatory Network n.d., Keller *et al* 2008, Schimel 2011). The number of qualifying stations within each region ranged from 51 (Northern Rockies) to 374 (Prairie Peninsula; figure S1).

Trends or changes in precipitation at the NEON-domain level are characterized using a trend-free pre-whitened form the regional Mann–Kendall trend test (Hussain and Mahmud 2019). The Mann–Kendall test is a widely used nonparametric statistical method for analyzing trends in climatological and hydrological time series data. Originally proposed by Mann (1945), it has since been extensively applied to environmental time series. This test offers two key advantages over other regression techniques: it does not require the data to follow a normal distribution, and it demonstrates low sensitivity to sudden changes caused by inhomogeneities within the time series. Mann-Kendall trend tests are thus suitable for detecting robust trends in hydrological time series (Hamed 2008) and are commonly used in studies assessing trends of precipitation over time (e.g. Roque-Malo and Kumar 2017, Panda and Sahu 2019, Zhang *et al* 2021, Harp and Horton 2023, Fattah *et al* 2024). Since annual trends are ultimately aggregates of seasonal patterns and trends, analyses are conducted on both annual and seasonal scales. The seasonal analyses presented herein are for the summer and winter seasons. We use four precipitation metrics to evaluate the ability of CMIP6 models to capture historical trends across the U.S. These metrics include changes in interannual precipitation variability, relative interannual variability (also known as coefficient of variation), annual mean precipitation, and annual wet day frequency, where a wet day is defined as a station day observing 1 mm or more of precipitation (a threshold common in precipitation analyses; e.g. Giorgi *et al* 2019). Here, we define interannual variability as the 11 year running standard deviation of annual precipitation; we use an 11 year window to lessen the impact of common modes of natural climate variability. We define relative interannual variability similarly, dividing the 11 year running standard deviation of annual precipitation (interannual variability) by the running mean of the same 11 year period. By doing so, the relative interannual variability accounts for changes in the interannual variability that are simply byproducts of shifting baselines of annual

mean precipitation. Collectively, these four variables either directly characterize interannual variability or provide crucial information to explain shifts in interannual variability (Harp and Horton 2023).

3. Results

3.1. Spatial distribution of annual and seasonal mean precipitation

We first assess the spatial distribution of observed annual mean precipitation across the 17 different NEON regions of the CONUS (figure S1). In the GHCN-D observations (figure 1(A)w), high values of annual mean precipitation (six regions $>$ 1,200 mm, nine regions $>$ 800 mm) are evident over the eastern CONUS, particularly in the U.S. southeast, while low values ($<$ 600 mm) dominate the western CONUS. The Pacific Northwest is an exception, where mean annual precipitation exceeds 1400 mm. The lowest mean precipitation is found over the Southern Rockies and Colorado Plateau, the Desert Southwest, and the Great Basin, each with less than 400 mm of precipitation annually.

Individual CMIP6 model single realizations (figure 1(A)a–u), along with the multi-model ensemble mean (referred to hereafter as 'EnsMean'; figure 1(A)v), reasonably capture the spatial distribution of the observed mean annual precipitation, albeit with varying magnitudes and noticeable biases. For instance, most CMIP6 ensemble members exhibit the lowest mean precipitation values in the Desert Southwest, while the Pacific Northwest generally exhibits the highest simulated values. In addition, almost all models, except for NorESM2-LM and NorESM2-MM, overestimate precipitation over most regions (10 of 16; figures 1(B) and S2(a)) while all models except for NESM3 underestimate precipitation over the Southeast. Most individual models demonstrate a pronounced overestimation (around twice the observed values) in the Great Basin and Northern Rockies regions (figures 1(B) and S2(b)). On the other hand, across the Southeast region, all of the selected models (except NESM3) exhibit a dry bias (indicated in red: figures 1(B) and S2(a)), with the MIROC6 model realization displaying the greatest negative bias (figure 1(B)) of approximately 20% (figure S2(b)). The CMIP6 models also reasonably represent the spatial distribution of observed mean summer (figure S3(A)) and winter (figure S4(A)) precipitation, despite notable biases (figures S3(B) and S4(B)) across different regions. In winter, the EnsMean shows a positive bias across all regions except the Southeast, with the largest positive bias observed in the Great Basin and Northern Rockies, exceeding 50 mm (figure S4(B-v)).

The 50-members of the CanESM5 SMILE likewise reasonably capture the spatial distribution of the observed mean annual precipitation (figure S5(a-xx)), with the ensemble mean of the CanESM5 realizations demonstrating remarkable fidelity with observed magnitudes (figure S5(yy)). However, most realizations (figure S6(a-xx)), along with the ensemble mean (figure S6(yy)), exhibit positive bias in eastern and western clusters of regions, such as in the Great Basin, Northern Rockies, Northeast and Mid Atlantic, while the Pacific Northwest depicts a negative bias in all CanESM5 realizations. In addition, the ensemble mean of CanESM5 (figure S6(yy)) exhibits a lower bias across most regions compared to the CMIP6 EnsMean (figure S6(zz)).

3.2. Trends in annual mean precipitation and wet day frequency

To properly contextualize changes in the interannual variability of precipitation, we first assess observed changes in annual, summer, and winter mean precipitation over all U.S. regions (figure 2(a)). We found increases in annual mean precipitation in most regions except over the Pacific Northwest and Northern Rockies, where a decrease is evident (figure 2(a)). The observed increases range from 5 to 22 mm decade^{-1}, with the largest increases ($>$20 mm decade^{-1}) occurring in regions east of the Rocky Mountains, such as Prairie Peninsula, Ozarks Complex, and Northeast. Observed decreasing trends exist within the Pacific Northwest and Northern Rockies regions, with values of -2 and -12 mm decade^{-1}, respectively. Seasonally, the observed trends in winter mean precipitation display a spatial pattern similar to that found in the annual mean, with increases generally in regions located east of the Rocky Mountains (figure 2(c)), except the Southeast and Mid Atlantic regions. Although this spatial pattern is less pronounced in summer (figure 2(b)), we identified some regions with greater precipitation increases (Prairie Peninsula, Southern Plains, and Northeast) in the summer ($\geqslant$5 mm decade^{-1}) compared to winter ($\sim$4 mm decade^{-1}).

To determine how well CMIP6 models capture precipitation trends, the magnitude of simulated trends from the models that comprise our CMIP6 multi-model ensemble are assessed against observed trends. The spatial patterns of annual mean precipitation trends in the EnsMean (figure S11v) largely mirror the spatial pattern in observed trends but generally underestimate the magnitude of the positive trends, especially over the Prairie Peninsula, Southern Plains, and Ozarks Complex regions. Individual models exhibit differing regional annual mean precipitation trend magnitudes (figure S11). Nevertheless, in 10 of 16 regions, at least 60% of the models agree with the sign of the observed annual mean precipitation change (figure 2(d)), with the highest agreement ($>$75%) evident over the Great Basin, Great Lakes, and Mid Atlantic regions. In the

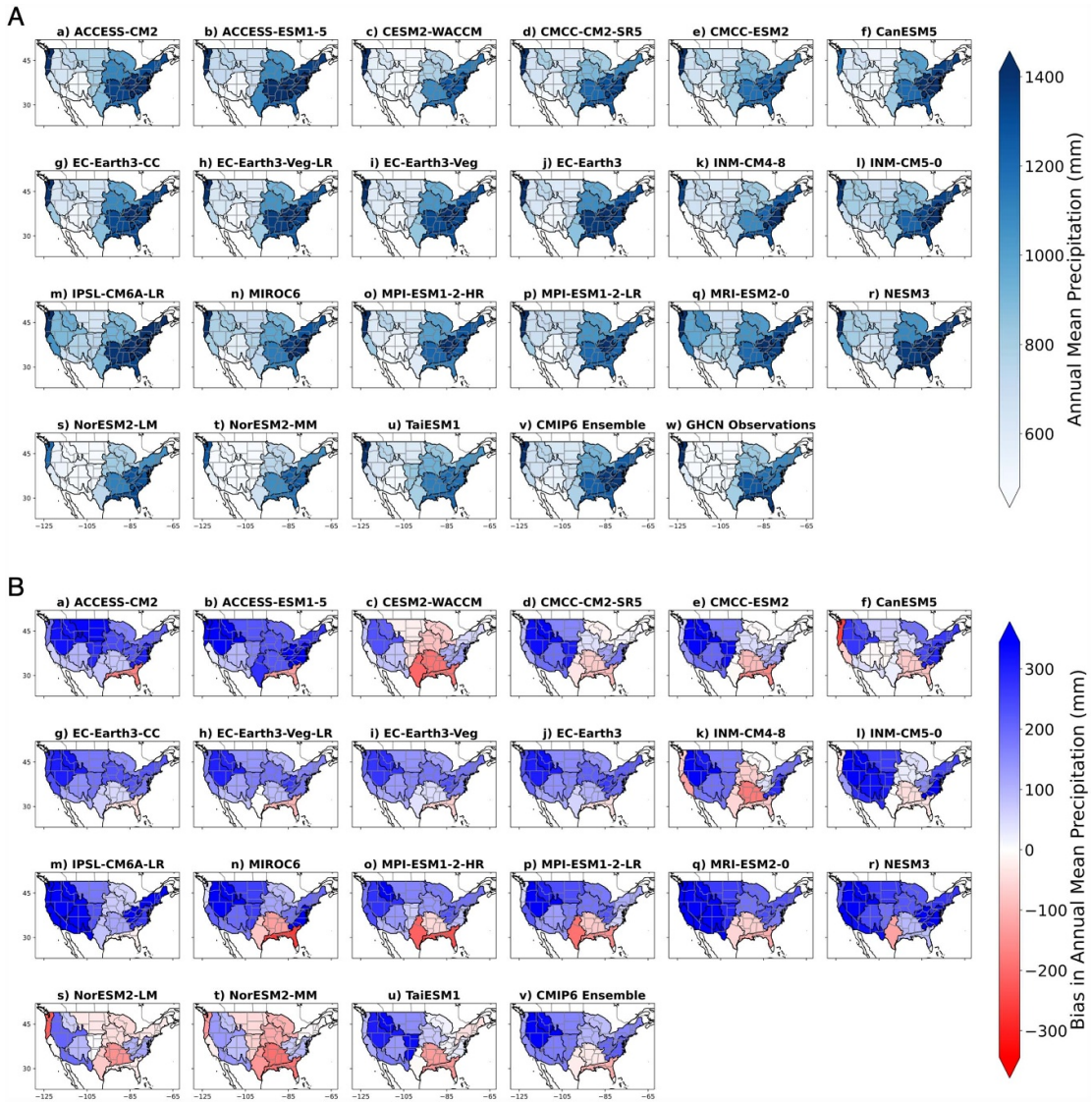

Figure 1. (A) Annual mean precipitation (mm) from 1951–2014 for (a-u) each included CMIP6 model (labeled), (v) the 21-member CMIP6 ensemble mean, and (w) the GHCN-D observations for each of 17 NEON domains (white-blue fill). (B) Bias in annual mean precipitation for each CMIP6 model (a-u) along with their ensemble mean (v) with respect to observations (red-blue fill).

Northern Rockies, fewer models (∼30%) agree with the sign of the observed change; this region exhibits the lowest inter-model agreement on the sign of observed changes. Seasonally, while over 75% of models agree on a decrease in summer precipitation in the Pacific Northwest, model agreement is generally low across most regions (figure 2(e)). In winter, however, inter-model agreement is higher in the northern regions and lower in the southern regions, with 76% agreement in the Great Lakes and just 43% agreement in the Southern Plains (figure 2(f)). Figures 2(g)–(i) further summarizes the spread of models' annual, summer and winter mean precipitation trends across different regions. The spread of the simulated annual trends is the smallest (largest) over the Pacific Northwest (Pacific Southwest) (figure 2(g)). This illustrates uncertainty in the simulated annual mean precipitation changes in the Pacific Southwest region, consistent with the low number of individual models (∼40%) that agree on the sign of the observed change (figure 2(d)). Although at least 50% of models agree on the sign of the observed change in the Prairie Peninsula, Ozarks Complex, and Northeast regions (figure 2(d)), the observed positive trends are largely underestimated by the majority of the CMIP6 models (figure 2(g)). In summer, the largest spread in the simulated precipitation trends is over the Southern Plains while in winter, it is observed over the Desert Southwest (figures 2(h) and (i)). Additionally, in winter, most models tend to underestimate the observed trends in these regions, which is consistent with the low agreement on the signs of the observed changes (figures 2(e)–(f)).

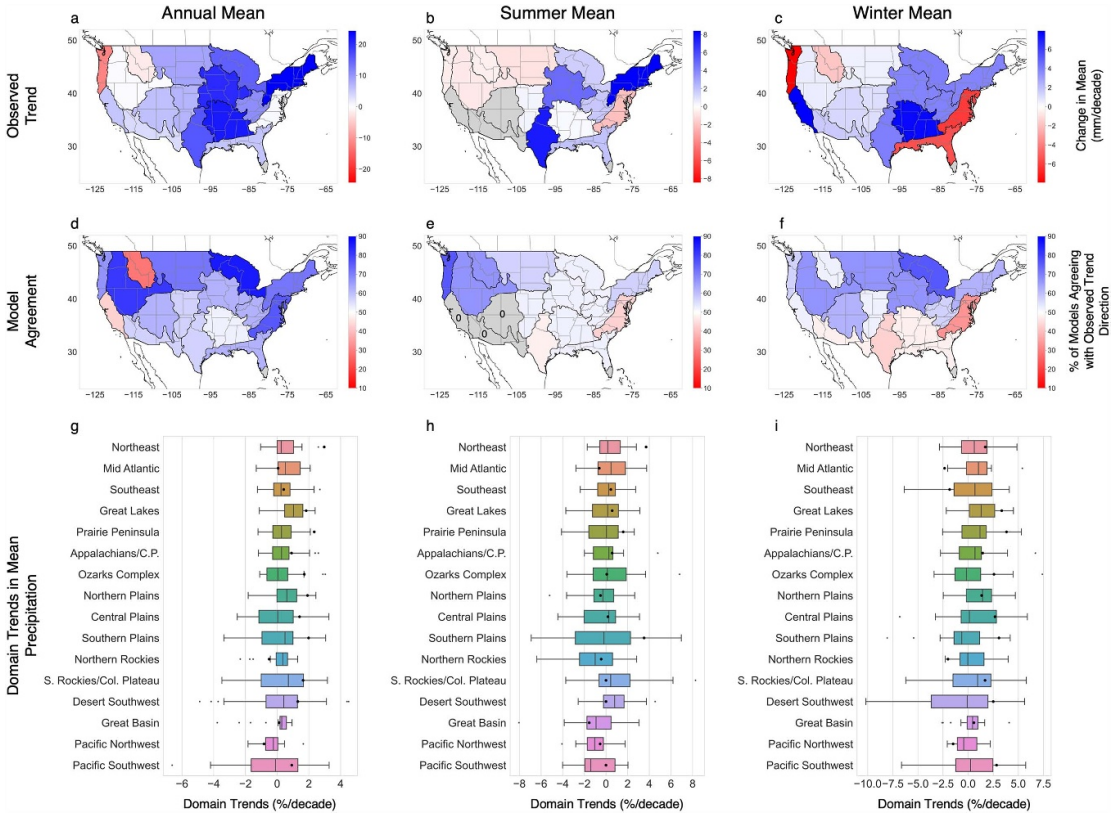

Figure 2. Trends in annual, summer, and winter mean precipitation. Observed precipitation trends in each NEON region from GHCN-D observations for (a) annual, (b) summer, and (c) winter precipitation (mm/decade; red-blue fill). Regions with no trend are shaded in gray. (d)–(f) The proportion of the 21 CMIP6 model ensemble that agree with the direction of the observed trends for (d) annual, (e) summer, and (f) winter precipitation (% of models; red-blue fill). The percentage of the CMIP6 model ensemble that agrees with no trend (gray) is indicated in text. (g)–(i) The spread of model-simulated trends in (g) annual, (h) summer, and (i) winter precipitation as a percentage of the corresponding annual or seasonal mean precipitation in observations for each NEON region (%/decade). Large black points mark trends in GHCN-D observations, smaller black points indicate CMIP6 model trends outliers.

Trends in annual, summer, and winter wet day frequency are presented in figure 3 for both GHCN-D observations and members of the CMIP6 multi-model ensemble. There are areas of pronounced increases in annual precipitation frequency in observations, with values exceeding 0.6 d decade^{-1} over the Great Lakes, Prairie Peninsula, and the Northeast regions (figure 3(a)). Conversely, decreasing trends in annual precipitation frequency (<-0.6 d decade^{-1}) dominate the Northern Rockies, Mid Atlantic, and Southeast regions. While many regions show negligible changes in precipitation frequency at both annual and seasonal scales (figures 3(a)–(c)), the observed annual increase in the Pacific Southwest, Great Lakes, and Prairie Peninsula aligns with positive trends in winter (figure 3(c)). In contrast, the annual increase in the Northeast is consistent with summer trends in the Northeast (figure 3(b)) although the change in wet day frequency during summer is minimal. Conversely, the decreases in annual precipitation frequency in the Pacific Northwest, Northern Rockies, Mid-Atlantic, and Southeast regions align with negative trends in winter (figure 3(c)). Generally, observed trends in wet day frequency were marginal, regardless of time frame.

The CMIP6 ensemble member-simulated trends in precipitation frequency vary widely (figure S12). For instance, CMCC-ESM2 and MRI-ESM2-0 exhibit increased annual precipitation frequency in almost all regions, whereas the NESM3 indicates the opposite. In general, the EnsMean trend of the models is consistent with observations from the Pacific Northwest, Northern Plains, Northern Rockies, Great Lakes, Northeast, and Prairie Peninsula, albeit with discrepancies in magnitude (figure S12v). Nevertheless, over 60% of the models agree with the observed trend over the Pacific Northwest, Northern Plains, and Great Lakes regions (figure 3(d)). This agreement was reduced to 50% over the Southern Rockies and Colorado Plateau and less than 40% over most other regions where non-zero trends are observed. In both summer and winter, the CMIP6 ensemble members largely exhibit low agreement (less than 40%) in regions where non-zero trends in precipitation frequency are observed (figures 3(e) and (f)). In general, most of the model simulations overestimate (underestimate) trends in annual precipitation frequency in the Mid Atlantic and Southeast (Prairie Peninsula) (figures 3(g)–(h) and S16(b)). However, the CMIP6 multi-model ensemble spread is relatively small in these regions. Conversely, simulated trends in precipitation frequency in the

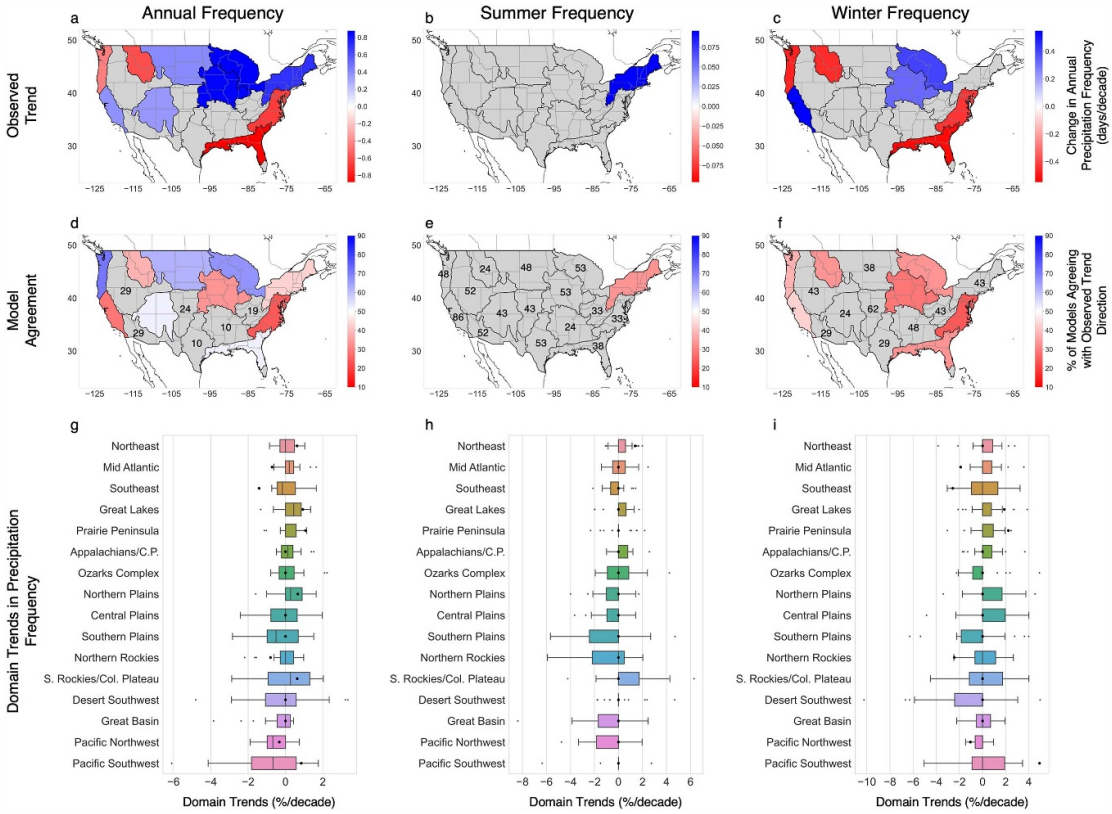

Figure 3. Trends in annual, summer, and winter precipitation frequency. Observed trends in precipitation frequency in each NEON region from GHCN-D observations for (a) annual, (b) summer, and (c) winter precipitation (mm/decade; red-blue fill). Regions with no trend are shaded in gray. (d)–(f) The proportion of the 21 CMIP6 model ensemble that agree with the direction of the observed trends for (d) annual, (e) summer, and (f) winter precipitation (% of models; red-blue fill). The percentage of the CMIP6 model ensemble that agrees with no trend (gray) is indicated in text. (g)–(i) The spread of model-simulated trends in (g) annual, (h) summer, and (i) winter precipitation frequency as a percentage of the corresponding annual or seasonal mean precipitation frequency in observations for each NEON region (%/decade). Large black points mark trends in GHCN-D observations, smaller black points indicate CMIP6 model trends outliers.

Southern Plains and Southern Rockies and Colorado Plateau regions have a large spread, suggesting potentially large structural uncertainties.

3.3. Trends in interannual precipitation variability

Given robust trends in observed annual precipitation and wet day frequency—as well as the mixed consistency on sign agreement with annual mean precipitation and wet day frequency trends within the CMIP6 multi-model ensemble—it is important to also assess whether precipitation variability has changed and is well captured by the CMIP6 multi-model ensemble. At the annual scale, we identify trends in observed interannual and relative interannual precipitation variability (figures 4(a) and S14(a)). We found a strong increase in the two metrics along the West Coast and northern East Coast, broadly speaking. The greatest observed increases exceed 8 mm decade^{-1} in interannual precipitation variability (Mid Atlantic and Pacific Northwest; figure 4(a)) and 0.01/decade in relative interannual precipitation variability (Pacific Northwest, Pacific Southwest, and Great Basin; Figure S14a). In summer (winter), regions located east (west) of the Rocky Mountains generally exhibit an increase in both metrics (figures 4(b) and (c), S14(b) and (c)). Nearly all regions exhibit a positive trend in relative interannual precipitation variability in summer (figure S14(b)).

The pattern of the simulated trends varies widely among CMIP6 ensemble members and from one region to another (figures S13, S15, S16(c) and (d)). However, by exhibiting reduced bias in most regions compared to individual CMIP6 model single realizations (figures S16(c) and (d)), the EnsMean captures the spatial pattern of the observed trends comparatively well, although the stronger increasing trends in coastal regions are underestimated (figures S13 and S15). Overall, about ∼60% of the ensemble members agree on the sign of observed change of interannual variability over the Great Basin, Central Plains, Southern Plains, and some eastern regions (figure 4(d)), while the Ozarks Complex depicts the lowest model agreement (∼30%). In summer (winter), the highest model agreement is exhibited in the Southeast (Northern Plains) region, while the lowest is in the Northern Plains (Northeast and Appalachians and Cumberland Plateau) (figures 4(e) and (f)). In most regions, the number of CMIP6 ensemble members agreeing on the observed sign of change in

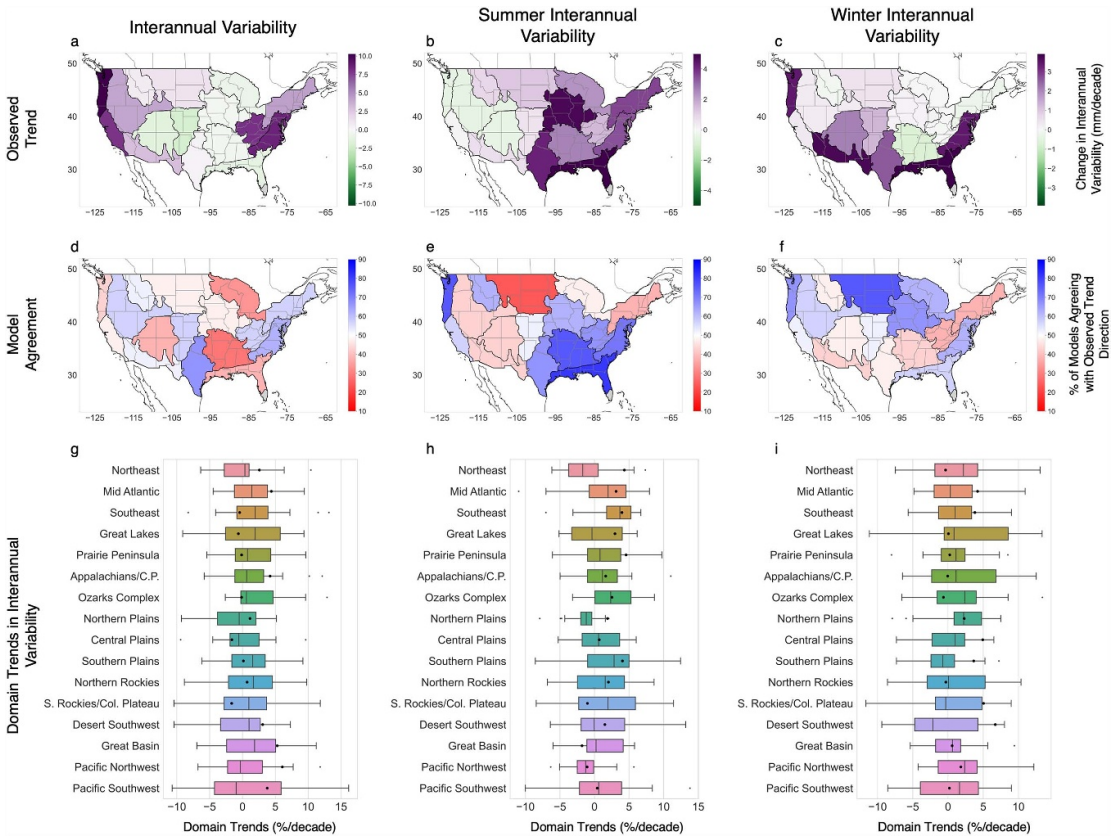

Figure 4. Trends in interannual variability of annual, summer, and winter precipitation. Observed trends in the interannual variability of precipitation in each NEON region from GHCN-D observations for (a) annual, (b) summer, and (c) winter precipitation (mm/decade; green-purple fill). (d)–(f) The proportion of the 21 CMIP6 model ensemble that agree with the direction of the observed trends for the interannual variability of (d) annual, (e) summer, and (f) winter precipitation (% of models; red-blue fill). (g)–(i) The spread of model-simulated trends in the interannual variability of (g) annual, (h) summer, and (i) winter precipitation as a percentage of the corresponding annual or seasonal mean interannual variability of precipitation in observations for each NEON region (%/decade). Large black points mark trends in GHCN-D observations, smaller black points indicate CMIP6 model trend outliers.

the relative interannual precipitation variability (figures S14(d) and (e)) mirrors that of interannual precipitation variability (figures 4(d) and (e)), albeit with some differences. For instance, the percentage agreement of interannual precipitation variability (figure 4(d)) is higher than that of relative interannual precipitation variability (figure S14(d)) in the Southern Plains. A similar pattern is observed in the Great Lakes during winter.

The spread of the CMIP6 ensemble member trends is also analyzed with respect to the observed trends (figures 4(g)–(i) and S14(g)–(i)). This spread is largest for both metrics of variability in the Great Lakes, Southeast, Southern Rockies and Colorado Plateau, and Pacific Southwest regions, with the spread between −10% to 15% in the Pacific Southwest (figures 4(g) and S14(g)). This highlights the uncertainty among annual CMIP6 ensemble member trends in those regions. In addition, the spread of winter trends is generally greater than in summer (figures 4(i) and S14(i)). Overall, trends in the four metrics show substantial regional variability across the U.S., with varying levels of regional spread among the CMIP6 ensemble members. This spread underscores potentially substantial model uncertainty, with some areas exhibiting weaker model agreement than others, especially regarding trends in precipitation frequency. To further contextualize this model uncertainty, we also examine the spread of realizations–or internal variability–within the CanESM5 large ensemble.

3.4. CanESM5 SMILE and the potential role of internal variability

Internal variability refers to the natural fluctuations that occur within the simulated climate system, arising from the intricate and chaotic interactions between the atmosphere, oceans, land, and ice (Blanusa *et al* 2023). This section assesses the contribution of internal variability in the interannual trends of precipitation over CONUS using the CanESM5_SMILE simulations. In figures 5 and S17, spatial patterns in annual mean precipitation and precipitation frequency trends vary between realizations. Despite this, CanESM5_SMILE mean trends are somewhat aligned with observed trends, though with reduced trend magnitudes (figure 5).

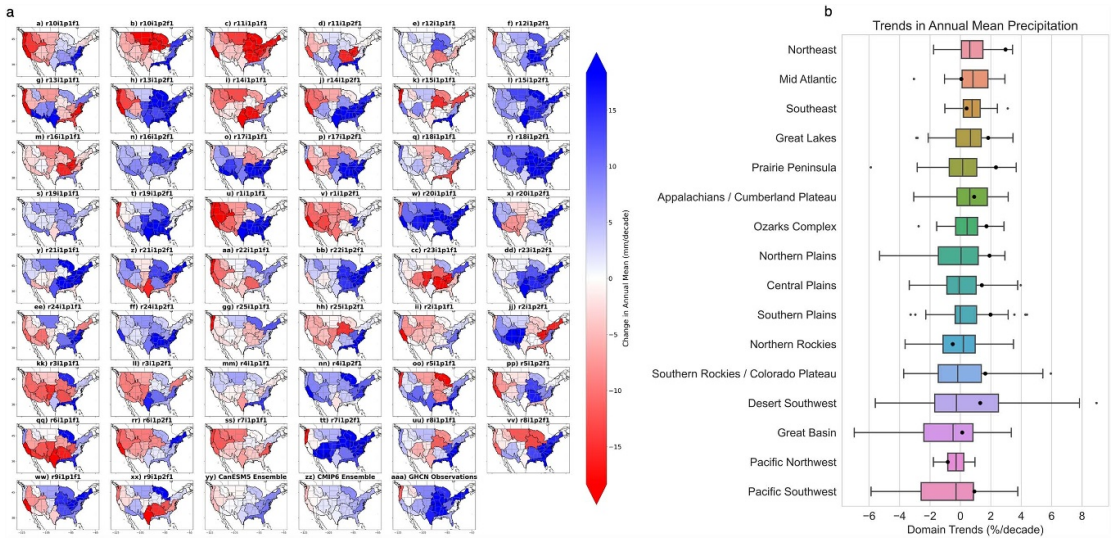

Figure 5. Trends in mean annual precipitation for CanESM5 SMILE. (a) Map of regional trends in annual mean precipitation for NEON regions for each CanESM5 SMILE model realization (a-xx; labeled), the ensemble mean of the CanESM5 large ensemble (yy), the ensemble mean of the CMIP6 model realizations (zz), and GHCN-D observations (aaa; mm/decade; red-blue fill). (b) The spread of annual mean precipitation trends across the 50 realizations of the CanESM5 SMILE as a percentage of the annual mean precipitation in GHCN-D observations for each NEON region (%/decade). Large black points represent the observed trends, while smaller points are outliers.

For example, the CanESM5_SMILE mean simulates an increase along the east coast of the CONUS, consistent with observations (figure 5(aaa)) and the CMIP6 EnsMean (figure 5(zz)). However, the CanESM5_SMILE mean indicates decreasing trends in the central and western U.S., which contrasts with widespread increases (central U.S.) and mixed trends (western U.S.) in observations.

The spread in annual mean precipitation and frequency trends from the 50 CanESM5 members is highest in the Desert Southwest, Southern Rockies and Colorado Plateau, Great Basin, and Pacific Southwest. A wider spread suggests greater internal variability in the simulated changes in those regions. Additionally, since internal variability tends to cancel out when averaging across members, the CanESM5_SMILE mean is used here to isolate the forced response (figures 5(yy) and S17(yy)). In most regions, the CanESM5_SMILE mean trend is smaller than that of individual realizations. This implies that trends in precipitation identified in individual ensemble members are a manifestation of the model's internal variability rather than a response to historical forcings.

The simulated annual trends in interannual and relative interannual precipitation variability of the 50 CanESM5_SMILE members and their ensemble mean are presented in figures S18 and S19, respectively. Their spatial pattern varies from one realization to another, with the largest spread in the trends of the 50 members observed in the Great Basin (interannual variability) and Pacific Southwest regions (relative interannual variability). Similar to the trends in mean precipitation and frequency, the magnitudes of the CanESM5_SMILE mean trends in interannual and relative interannual precipitation variability are low in all the regions compared to that of individual ensemble realization. As explained above, this indicates that model internal variability likely dominates total uncertainty in the simulated trends. To demonstrate the consequences of this finding, we plot the ratio of the spread of CanESM SMILE realization trends to that of the CMIP6 multi-model ensemble trends for both interannual and relative interannual precipitation variability (figures 6(c) and (d)). We find that in many NEON regions, the spread of the CanESM5 SMILE-simulated trends in internal variability is equal to or exceeds the spread of the CMIP6 multi-model ensemble trends.

4. Discussion and summary

Evaluating the historical performance of CMIP6 models is crucial for understanding the impacts of climate change on hydrological cycles and precipitation patterns. Numerous studies (e.g. Agel and Barlow 2020, Srivastava *et al* 2020, Akinsanola *et al* 2020b, Wang and Asefa 2024) have evaluated the ability of CMIP6 models to represent the historical mean and extreme precipitation in the U.S. However, despite its significance for climate impact studies and policy-making, the interannual variability of precipitation has not been thoroughly evaluated. To address this gap, this study analyzes interannual precipitation variability

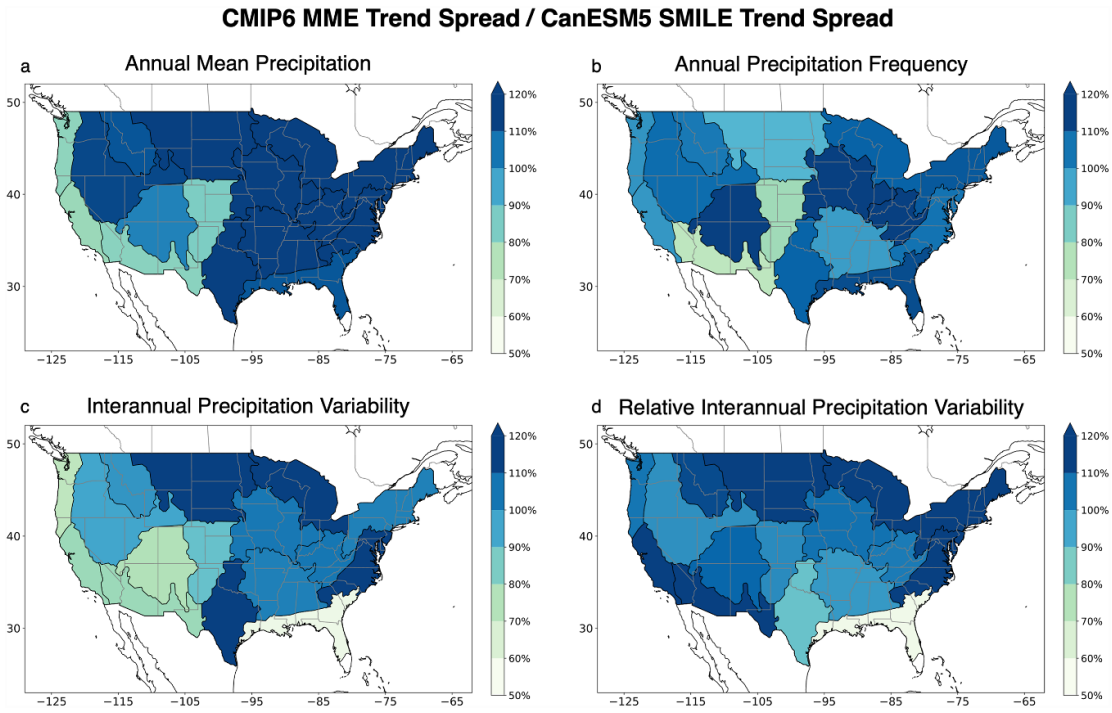

Figure 6. Percent of the variability in CMIP6 model trends in annual mean precipitation (a), precipitation frequency (b), interannual variability (c), and relative interannual variability (d) spanned by the CanESM5 SMILE trends. These values are calculated by dividing the difference between the maximum and minimum trend values in the CanESM5 SMILE with the difference between the maximum and minimum trend values in the CMIP6 multi-model ensemble for each region.

across the contiguous U.S., utilizing observational data and outputs from CMIP6 models at both annual and seasonal scales. By employing regional Mann-Kendall trend tests, we examined trends in four key precipitation metrics: interannual precipitation variability, relative interannual variability, annual mean precipitation, and annual wet day frequency. Our analysis covered 17 climatically homogeneous domains, providing valuable insights into the ability of CMIP6 models to replicate observed precipitation patterns. We also use the 50-member CanESM5 SMILE simulations to provide context on the role of internal variability when identifying observed trends in CMIP6 model simulations.

Our results reveal a general increase in observed annual mean precipitation across most regions, though with notable regional variations in trends. The most significant increases occurred east of the Rocky Mountains. The observed trends in winter mean precipitation broadly exhibit a spatial pattern similar to that of the annual mean, except in the southeast U.S., where the spatial pattern in summer differs from that of winter. This finding agrees with that of Wang *et al* (2021), who demonstrated that summer total precipitation in southeastern regions of CONUS is tied to accumulated cyclone energy (ACE) and therefore cyclone season, whereas winter total precipitation in this area is strongly linked to El Niño-Southern Oscillation (ENSO).

While the CMIP6 ensemble members generally reproduced the spatial patterns of mean annual precipitation trends, discrepancies in magnitude were evident. However, at both annual and seasonal scales, CMIP6 members demonstrated modest to good agreement with the signs of observed changes in most regions except for winter in the Southern Plains, where agreement is 43% (figure 2(f)). Low agreement may be attributable to the inherent challenges in accurately simulating large-scale processes that govern precipitation interannual variability, such as the ENSO (Huang 2016). Conversely, ensemble members typically exhibited low agreement with the signs of observed changes for the simulated trends in wet day frequency, particularly in winter. Previous studies have shown that changes in mean precipitation are driven by changes in wet day frequency, daily precipitation intensity, or a combination of both (Harp and Horton 2023). Our findings suggest that a model's ability to replicate observed changes in mean precipitation accurately may be associated with their proficiency in replicating changes in daily precipitation intensity, as most models fail to simulate the signs of observed changes in wet day frequency.

Both interannual and relative interannual precipitation variability exhibit increases along the West Coast and Northeast in observations. These changes may be associated with the variability of inland moisture penetration from neighboring oceans (Hoerling *et al* 2016) since the trend is not evident in the interior U.S. In addition, the annual increase in interannual precipitation variability observed over the Pacific Northwest (Northeast) aligns with, and may be driven by, winter (summer) trends (figures 4(a)–(c)). Our analysis

revealed that individual CMIP6 ensemble members struggle to accurately capture the broad spatial patterns and magnitude of trends in interannual variability when compared to observational data. Similarly, the EnsMean did not successfully replicate spatial patterns in relative interannual variability trends. This may be partly due to an inability to capture changes in frequency. For instance, in the Pacific Southwest, few ensemble members agreed on the signs of observed changes in interannual precipitation variability, which coincides with their inability to simulate changes in wet day frequency. Despite this potential physics-based explanation, it is important to note that while no individual CMIP6 ensemble member, nor the ensemble mean, replicates the observed trend magnitudes in all NEON domains, all observed trend magnitudes in all regions are captured within the ensemble spread, typically within the interquartile range (figures 4(g)–(i)).

The role of internal variability in climate model simulations has been shown to be substantial and comparable to externally forced responses (Deser *et al* 2020). Previous studies have demonstrated that the distribution of continental-to-regional scale trends from a climate variable created using a CMIP ensemble can be narrower in magnitude than a distribution created from a SMILE (Mankin *et al* 2015, 2020, Deser *et al* 2020, Lehner and Deser 2023). Thus, a CMIP6 multi-model ensemble, particularly one that uses only a single realization from each model like that employed in the present study, may underpredict internal/natural variability. Consequently, its distribution may be less likely than a SMILE to include the observed trend and may improperly characterize uncertainty in results. Our results have demonstrated that internal variability, as captured by the 50-member CanESM5 SMILE, may account for much of the inter-model variability within the CMIP6 ensemble. In agreement with the findings from Mankin *et al* (2015, 2020), this indicates that internal climate variability may account for a large part of the multi-model uncertainty. However, we acknowledge that model-simulated internal variability in SMILEs can suffer from both under- and over-estimation of natural variability and that these biases may differ regionally (Suarez-Gutierrez *et al* 2021). We likewise acknowledge that our findings could differ if a SMILE for each of the 21 CMIP6 models were utilized. Cumulatively, these points suggest that efforts to improve the skill of individual models and, thus, reduce structural uncertainties, may be limited both by irreducible uncertainties and limited/biased estimates of natural variability.

We caveat our study methodology by first noting that comparing station observations against climate model output has limitations, even when data are regionally aggregated. For instance, while we regrid CMIP6 outputs onto a common grid to allow for direct model comparison, the resultant number of climate model data points is limited and may not be truly representative of the underlying precipitation patterns (figure S1). Additionally, despite the much denser network of station observations within the U.S. compared to our common climate model grid, the placement of rain gauges is often near cities or other points of socioeconomic importance (e.g. airports) and is not evenly distributed spatially throughout regions (Villarini *et al* 2008). This is particularly true in sparsely populated and mountainous areas. Thus, while aggregating at a climatically-informed regional scale allows for a more robust trend analysis of individual station data records, the inconsistent distribution of gauge networks may overrepresent particular areas within regions, and some regions may possess limited station availability. This may also introduce discrepancies with our climate model output as data are confined to their underlying grid regardless of the underlying climatological features. We also assume that the NEON domains we use here possess internally consistent climate—as they are designed by construction—but domain boundaries are inevitably imperfect and within-domain variability persists. Additionally, trends for one region (Atlantic Neotropical) are not characterized here as the small region is not represented in the common grid. Finally, although regridding climate model output is the best way to allow comparison, this process can introduce systematic bias (Rajulapati *et al* 2021).

While this study has provided valuable insights into precipitation trends and interannual variability within the CanESM5 SMILE and CMIP6 historical multi-model ensemble, there are several remaining avenues for advancing this work. One promising direction would disentangle forced trends from internal variability by utilizing the accompanying pre-industrial control (piControl) simulations. For example, splitting the CanESM5 piControl into segments paralleling the historical ensemble members would allow for a direct comparison of the forced trends with internal variability alone. This approach would provide statistical and practical significance to the trends observed in the historical runs and contextualize them relative to internal variability as simulated by CanESM5. Extending this analysis to the CMIP6 multi-model ensemble by using the piControl runs of each participating model would further enhance understanding of forced trends and variability across a broader range of models. Such a formal attribution framework could isolate the role of external forcing on precipitation variability and trends, offering insights critical for improving model simulations and guiding climate adaptation strategies. In addition to exploring forced and internal variability, future studies could also investigate variability on shorter timescales, such as sub-seasonal or daily precipitation accumulations. These analyses would provide a more comprehensive understanding of the drivers of precipitation variability, particularly in the context of extreme events, and complement the interannual variability focus of this study. Building on the results presented here, these

follow-up analyses could yield a more complete picture of precipitation variability and its underlying mechanisms, representing important steps toward more robust climate modeling and prediction efforts.

Foreknowledge of expected precipitation is critical to a number of water resource-dependent fields. From agricultural crop yields to hydroelectric power generation to lake level dependent recreation, the ability to plan for, and build according to, a climatological expectation is both economically and infrastructurally essential (Rowhani *et al* 2011, Sloat *et al* 2018, Boadi and Owusu 2019, Shortridge 2019, Qin *et al* 2020, Gronewold *et al* 2021). Given the importance of this foreknowledge, building confidence in both model projections and their underlying uncertainties via analyses of model replication of historical trends is needed. Our study highlights opportunities for improvement in simulating precipitation variability using CMIP6 models. All told, we find evidence of model skill as well as opportunities for model improvement. Our results show the CMIP6 multi-model ensemble demonstrates some skill in capturing broad-scale spatial patterns in trends in annual precipitation, though discrepancies in magnitude and regional trends are prevalent. Additionally, while we find an inability of the CMIP6 multi-model ensemble to reproduce observed trends in the other precipitation metrics examined in aggregate, observed trends do predominately lie within the spread of the CMIP6 multi-model ensemble, indicating that individual ensemble members possess the ability to replicate trends in interannual variability. While these results underscore the need for ongoing model refinement, validation, and examination in the context of internal variability, we note that efforts to advance these model aspects may be constrained by irreducible uncertainty of internal variability. Ultimately, addressing these issues is crucial for improving the accuracy of climate projections, especially in regions vulnerable to extreme precipitation events and variability.

Data availability statement

The data that support the findings of this study are openly available at the following URL/DOI: www.ncei.noaa.gov/products/land-based-station/global-historical-climatology-network-daily;https://esgf.llnl.gov/.

Acknowledgment

We thank the National Centers for Environmental Information for publicly sharing the GHCN-D data set. We extend our gratitude to the World Climate Research Programme's Working Group on Coupled Modeling, the entity behind CMIP, and we appreciate the climate modeling groups (models detailed in table S1) for producing and making available their model outputs.D E H acknowledges support from NSF PREESENTS Grant No. 1854951.

Funding

Ryan D Harp and Daniel E Horton were supported by NSF PREEVENTS Grant No. 1854951 awarded to DEH.

ORCID iDs

Ryan D Harp https://orcid.org/0000-0002-2872-8541
Thierry N Taguela https://orcid.org/0000-0001-8140-125X
Akintomide A Akinsanola https://orcid.org/0000-0002-0192-0082
Daniel E Horton https://orcid.org/0000-0002-2065-4517

References

Abghari H, Tabari H and Hosseinzadeh Talaee P 2013 River flow trends in the west of Iran during the past 40 years: impact of precipitation variability *Glob. Planet. Change* **101** 52–60

Agel L and Barlow M 2020 How well do CMIP6 historical runs match observed Northeast U.S. precipitation and extreme precipitation–related circulation? *J. Clim.* **33** 9835–48

Akinsanola A A, Kooperman G J, Pendergrass A G, Hannah W M and Reed K A 2020b Seasonal representation of extreme precipitation indices over the United States in CMIP6 present-day simulations *Environ. Res. Lett.* **15** 104078

Akinsanola A A, Kooperman G J, Reed K A, Pendergrass A G and Hannah W M 2020c Projected changes in seasonal precipitation extremes over the United States in CMIP6 simulations *Environ. Res. Lett.* **15** 104078

Akinsanola A A, Zhou W, Zhou T and Keenlyside N 2020a Amplification of synoptic to annual variability of West African summer monsoon rainfall under global warming *npj Clim. Atmos. Sci.* **3** 21

Alexander L V *et al* 2006 Global observed changes in daily climate extremes of temperature and precipitation *J. Geophys. Res.* **111** D05109

Barlow M, Nigam S and Berbery E H 2001 ENSO, Pacific decadal variability, and U.S. summertime precipitation, drought, and stream flow *J. Clim.* **14** 2105–28

Blanusa M L, López-Zurita C J and Rasp S 2023 Internal variability plays a dominant role in global climate projections of temperature and precipitation extremes *Clim. Dyn.* **61** 1931–45

Boadi S A and Owusu K 2019 Impact of climate change and variability on hydropower in Ghana *Afr. Geogr. Rev.* **38** 19–31
Bobde V, Akinsanola A A, Folorunsho A H, Adebiyi A A and Adeyeri O E 2024 Projected regional changes in mean and extreme precipitation over Africa in CMIP6 models *Environ. Res. Lett.* **19** 074009
Corringham T W, Ralph F M, Gershunov A, Cayan D R and Talbot C A 2019 Atmospheric rivers drive flood damages in the western United States *Sci. Adv.* **5** eaax4631
Deser C, Lehner F, Rodgers K B, Ault T, Delworth T L, DiNezio P N and Ting M 2020 Insights from Earth system model initial-condition large ensembles and future prospects *Nat. Clim. Change* **10** 277–86
Durre I, Menne M J, Gleason B E, Houston T G and Vose R S 2010 Comprehensive automated quality assurance of daily surface observations *J. Appl. Meteorol. Climatol.* **49** 1615–33
Eyring V, Bony S, Meehl G A, Senior G A, Stevens B, Stouffer R J and Taylor K E 2016 Overview of the coupled model intercomparison project phase 6 (CMIP6) experimental design and organization *Geosci. Model. Dev.* **9** 1937–58
Fattah M A, Hasan M M, Dola I A, Morshed S R, Chakraborty T, Kafy A A, Alsulamy S, Khedher K M and Shohan A A A 2024 Implications of rainfall variability on groundwater recharge and sustainable management in South Asian capitals: an in-depth analysis using Mann Kendall tests, continuous wavelet coherence, and innovative trend analysis *Groundwater Sustain. Dev.* **24** 101060
Furtak K and Wolińska A 2023 The impact of extreme weather events as a consequence of climate change on the soil moisture and on the quality of the soil environment and agriculture—a review *Catena* **231** 107378
Giorgi F, Raffaele F and Coppola E 2019 The response of precipitation characteristics to global warming from climate projections *Earth Syst. Dyn.* **10** 73–89
Griffin D and Anchukaitis K J 2014 How unusual is the 2012–2014 California drought? *Geophys. Res. Lett.* **41** 9017–23
Groisman P Y, Knight R W and Karl T R 2012 Changes in intense precipitation over the central United States *J. Hydrometeorol.* **13** 47–66
Gronewold A D, Do H X, Mei Y and Stow C A 2021 A tug-of-war within the hydrologic cycle of a continental freshwater basin *Geophys. Res. Lett.* **48** e2020GL090374
Hamed K H 2008 Trend detection in hydrologic data: the Mann–Kendall trend test under the scaling hypothesis *J. Hydrol.* **349** 350–63
Harp R D and Horton D E 2022 Observed changes in daily precipitation intensity in the United States *Geophys. Res. Lett.* **49** e2022GL099955
Harp R D and Horton D E 2023 Observed changes in interannual precipitation variability in the United States *Geophys. Res. Lett.* **50** e2023GL104533
Hoerling M, Eischeid J, Perlwitz J, Quan X W, Wolter K and Cheng L 2016 Characterizing recent trends in U.S. heavy precipitation *J. Clim.* **29** 2313–32
Huang P 2016 Time-varying response of ENSO-induced tropical pacific rainfall to global warming in CMIP5 models. Part I: multimodel ensemble results *J. Clim.* **29** 5763–78
Hussain M and Mahmud I 2019 pyMannKendall: a python package for non parametric Mann Kendall family of trend tests *J. Open Source Softw.* **4** 1556
Karl T R and Knight R W 1998 Secular trends of precipitation amount, frequency, and intensity in the United States *Bull. Am. Meteorol. Soc.* **79** 231–41
Keller M, Schimel D S, Hargrove W W and Hoffman F M 2008 A continental strategy for the national ecological observatory network *Ecol. Soc. Am.* **6** 282–4
Kunkel K E *et al* 2013 Monitoring and understanding trends in extreme storms: state of knowledge *Bull. Am. Meteorol. Soc.* **94** 499–514
Lehner F and Deser C 2023 Origin, importance, and predictive limits of internal climate variability *Environ. Res. Clim.* **2** 023001
Lehner F, Deser C, Maher N, Marotzke J, Fischer E M, Brunner L, Knutti R and Hawkins E 2020 Partitioning climate projection uncertainty with multiple large ensembles and CMIP5/6 *Earth Syst. Dyn.* **11** 491–508
Li L, Li W and Barros A P 2013 Atmospheric moisture budget and its regulation of the summer precipitation variability over the Southeastern United States *Clim. Dyn.* **41** 613–31
Mankin J S, Lehner F, Coats S and McKinnon K A 2020 The value of initial condition large ensembles to robust adaptation decision-making *Earth's Future* **8** e2012EF001610
Mankin J S, Viviroli D, Singh D, Hoekstra A Y and Diffenbaugh N S 2015 The potential for snow to supply human water demand in the present and future *Environ. Res. Lett.* **10** 114016
Mann H B 1945 Nonparametric tests against trend *Econometrica* **13** 245
Masson-Delmotte V *et al* 2021 Climate change 2021: the physical science basis *Contribution of Working Group I to the Sixth Assessment Report of the Intergovernmental Panel on Climate Change* (IPCC)
Meehl G A, A C, Eyring V, Flato G, Lamarque J F, Stouffer R J, Taylor K E and Schlund M 2020 Context for interpreting equilibrium climate sensitivity and transient climate response from the CMIP6 earth system models *Sci. Adv.* **6** eaba1981
Menne M J, Durre I, Vose R S, Gleason B E and Houston T G 2012 An overview of the global historical climatology network-daily database *J. Atmos. Ocean. Technol.* **29** 897–910
Nash D, Ye H and Fetzer E 2017 Spatial and temporal variability in winter precipitation across the Western United States during the satellite era *Remote Sens.* **9** 928
National Ecological Observatory Network n.d. *Spatial and Temporal Design. NEON Science.* (available at: https://www.neonscience.org/about/overview/design) (Accessed 27 November 2024)
Panda A and Sahu N 2019 Trend analysis of seasonal rainfall and temperature pattern in Kalahandi, Bolangir and Koraput districts of Odisha, India *Atmos. Sci. Lett.* **20** e932
Pendergrass A G and Hartmann D L 2014 The atmospheric energy constraint on global-mean precipitation change *J. Clim.* **27** 757–68
Peterson T C *et al* 2013 Monitoring and understanding changes in heat waves, cold waves, floods, and droughts in the United States: state of Knowledge *Bull. Am. Meteorol. Soc.* **94** 821–34
Polade S D, Pierce D W, Cayan D R, Gershunov A and Dettinger M D 2014 The key role of dry days in changing regional climate and precipitation regimes *Sci. Rep.* **4** 1–8
Qin P, Xu H, Liu M, Du L, Xiao C, Liu L and Tarroja B 2020 Climate change impacts on three Gorges reservoir impoundment and hydropower generation *J. Hydrol.* **580** 123922
Qiu H, Zhou T, Chen X, Wu B and Jiang J 2024 Understanding the diversity of CMIP6 models in the projection of precipitation over Tibetan Plateau *Geophys. Res. Lett.* **51** e2023GL106553
Rajulapati C R, Papalexiou S M, Clark M P and Pomeroy J W 2021 The perils of regridding: examples using a global precipitation dataset *J. Appl. Meteorol. Climatol.* **60** 1561–73

Riha S J, Wilks D S and Simoens P 1996 Impact of temperature and precipitation variability on crop model predictions *Clim. Change* **32** 293–311
Rivera J A and Arnould G 2020 Evaluation of the ability of CMIP6 models to simulate precipitation over Southwestern South America: climatic features and long-term trends (1901–2014) *Atmos. Res.* **241** 104953
Roque-Malo S and Kumar P 2017 Patterns of change in high frequency precipitation variability over North America *Sci. Rep.* **7** 1–12
Rowell D P 2019 An observational constraint on CMIP5 projections of the East African long rains and Southern Indian ocean warming *Geophys. Res. Lett.* **46** 6050–8
Rowhani P, Lobell D B, Linderman M and Ramankutty N 2011 Climate variability and crop production in Tanzania *Agric. For. Meteorol.* **151** 449–60
Schimel D 2011 The era of continental-scale ecology *Front. Ecol. Environ.* **9** 311
Shortridge J 2019 Observed trends in daily rainfall variability result in more severe climate change impacts to agriculture *Clim. Change* **157** 429–44
Sloat L L, Gerber J S, Samberg L H, Smith W K, Herrero M, Ferreira L G, Godde C M and West P C 2018 Increasing importance of precipitation variability on global livestock grazing lands *Nat. Clim. Change* **8** 214–8
Srivastava A, Grotjahn R and Ullrich P A 2020 Evaluation of historical CMIP6 model simulations of extreme precipitation over contiguous US regions *Weather Clim. Extremes* **29** 100268
Stevenson S, Timmermann A, Chikamoto Y, Langford S and DiNezio P 2015 Stochastically generated North American Megadroughts *J. Clim.* **28** 1865–80
Suarez-Gutierrez L, Milinski S and Maher N 2021 Exploiting large ensembles for a better yet simpler climate model evaluation *Clim. Dyn.* **57** 2557–80
Swart N C *et al* 2019 The Canadian earth system model version 5 (CanESM5.0.3) *Geosci. Model. Dev.* **12** 4823–73
Taguela T N, Pokam W M and Washington R 2022 Rainfall in uncoupled and coupled versions of the met office unified model over Central Africa: investigation of processes during the September–November rainy season *Int. J. Climatol.* **42** 6311–31
U.S. Global Change Research Program 2023 *5th National Climate Assessment* ed A R Crimmins, C W Avery, D R Easterling, K E Kunkel, B C Stewart and T K Maycock (U.S. Global Change Research Program) (https://doi.org/10.7930/NCA5.2023)
Villarini G, Mandapaka P V, Krajewski W F and Moore R J 2008 Rainfall and sampling uncertainties: a rain gauge perspective *J. Geophys. Res. Atmos.* **113** D11102
Wang H and Asefa T 2024 Enhanced performance of CMIP6 climate models in simulating historical precipitation in the Florida Peninsula *Int. J. Climatol.* **44** 2758–78
Wang H, Asefa T and Erkyihun S 2021 Interannual variabilities of the summer and winter extreme daily precipitation in the Southeastern United States *J. Hydrol.* **603** 127013
Williams A P, Cook B I and Smerdon J E 2022 Rapid intensification of the emerging southwestern North American megadrought in 2020–2021 *Nat. Clim. Change* **12** 232–4
Wood R R, Lehner F, Pendergrass A G and Schlunegger S 2021 Changes in precipitation variability across time scales in multiple global climate model large ensembles *Environ. Res. Lett.* **16** 084022
Wood R R and Ludwig R 2020 Analyzing internal variability and forced response of subdaily and daily extreme precipitation over Europe *Geophys. Res. Lett.* **47** e2020GL089300
Zhang F, Biederman J A, Dannenberg M P, Yan D, Reed S C and Smith W K 2021 Five decades of observed daily precipitation reveal longer and more variable drought events across much of the western United States *Geophys. Res. Lett.* **48** e2020GL092293